Science Translational Medicine
AAAS

Rapid Cancer Detection by Topically Spraying a γ-Glutamyltranspeptidase–Activated Fluorescent Probe

Yasuteru Urano *et al.*

Sci Transl Med **3**, 110ra119 (2011);
DOI: 10.1126/scitranslmed.3002823

Editor's Summary

No Tumor Left Behind

Although quick action with spray paint usually conjures images of a schoolboy prank, researchers now show that spray painting of tiny tumors might save lives by illuminating these troublemakers that are often overlooked by the naked eye.

Ovarian cancer is a deadly gynecological disease, considering its propensity for invading the peritoneal cavity and depositing tumors throughout. Surgeons can miss these disseminated tumors during surgical removal of cancerous lesions, owing to their small size (~1 mm) and unclear borders. To help surgeons visualize and eliminate these clandestine killers, Urano *et al*. have developed a small-molecule aminopeptidase probe that fluoresces upon contact with cancer cells. The probe ––γ-glutamyl hydroxymethyl rhodamine green (gGlu-HMRG)––is intramolecularly caged, so that it is quenched (nonfluorescent) in its "off" state. When the probe encounters cancer cells, which overexpress the enzyme γ-glutamyltranspeptidase (GGT), the gGlu is cleaved, simultaneously turning "on" the fluorescent HMRG. Urano and colleagues first tested the probe in 11 human ovarian cancer cell lines in vitro and observed rapid fluorescence within 10 min after addition of the imaging agent to the cell cultures. They next moved into several mouse models of disseminated human peritoneal ovarian cancer, using a spray formulation of the probe that allowed the researchers to topically apply the probe during surgery or endoscopy. Within 1 min of spraying the tumors, gGlu-HMRG was enzymatically cleaved, revealing a bright fluorescent region of the peritoneal cavity in which the cancerous lesions were located. These small nodules were quickly and completely removed from living animals with forceps, demonstrating the power of rapid fluorescence-guided tumor resection.

This gGlu-based fluorescent probe as well as several other aminopeptidase–based reagents identified by the authors could help surgeons to track down tiny tumors dispersed throughout body cavities, ensuring that no residual tumor is left behind. Complete obliteration of disseminated tumors should improve cancer outcomes after surgery.

Science Translational Medicine (print ISSN 1946-6234; online ISSN 1946-6242) is published weekly, except the last week in December, by the American Association for the Advancement of Science, 1200 New York Avenue NW, Washington, DC 20005.

CANCER IMAGING

Rapid Cancer Detection by Topically Spraying a γ-Glutamyltranspeptidase–Activated Fluorescent Probe

Yasuteru Urano,[1,2]* Masayo Sakabe,[3] Nobuyuki Kosaka,[4] Mikako Ogawa,[4] Makoto Mitsunaga,[4] Daisuke Asanuma,[1] Mako Kamiya,[1] Matthew R. Young,[5] Tetsuo Nagano,[3] Peter L. Choyke,[4] Hisataka Kobayashi[4]*

The ability of the unaided human eye to detect small cancer foci or accurate borders between cancer and normal tissue during surgery or endoscopy is limited. Fluorescent probes are useful for enhancing visualization of small tumors but are typically limited by either high background signal or the requirement for administration hours to days before use. We synthesized a rapidly activatable, cancer-selective fluorescence imaging probe, γ-glutamyl hydroxymethyl rhodamine green (gGlu-HMRG), with intramolecular spirocyclic caging for complete quenching. Activation occurs by rapid one-step cleavage of glutamate with γ-glutamyltranspeptidase (GGT), which is not expressed in normal tissue, but is overexpressed on the cell membrane of various cancer cells, thus leading to complete uncaging and dequenching of the fluorescence probe. In vitro activation of gGlu-HMRG was evident in 11 human ovarian cancer cell lines tested. In vivo in mouse models of disseminated human peritoneal ovarian cancer, activation of gGlu-HMRG occurred within 1 min of topically spraying the tumor, creating high signal contrast between the tumor and the background. The gGlu-HMRG probe is practical for clinical application during surgical or endoscopic procedures because of its rapid and strong activation upon contact with GGT on the surface of cancer cells.

INTRODUCTION

Successful oncologic procedures rely on the rapid and accurate localization of cancerous tissues followed by their complete resection or ablation. Although large tumors are visible to the unaided human eye, tiny foci (2 to 3 mm) of cancer metastases or invading cells may be impossible to see. Optical fluorescence molecular imaging has been investigated as an aid to optically guided surgery (*1*) and endoscopy (*2*) because of its high sensitivity, low cost, portability, real-time capabilities, and, importantly, absence of ionizing radiation (*3*). There are two major categories of fluorescent probes that have been used in this setting: "always on" and activatable (*4*). Always-on probes have the disadvantage of high background signal, which requires considerable time to clear to achieve adequate target-to-background ratios (TBRs). Activatable probes have lower background signals, but the activation process often requires hours to days, which decreases their practicality for routine or real-time clinical use (*5*). For instance, we have developed activatable fluorescence probes with antibodies against epidermal growth factor receptors (*6*, *7*) and with glycoprotein ligands against lectins (*6*, *8*). These cancer-specific probes fluoresced after binding to specific cell surface receptors—a process that could take at least 1 hour to achieve an adequate TBR.

Other activatable probes are based on the dequenching of a fluorescent molecule after proteolysis of its peptide backbone, which hold the fluorophores in a quenched state. Peptide sequences that are substrates for enzymes such as cathepsin and matrix metalloproteinase (MMP), which are commonly found in the microenvironment of tumors, have been used for this purpose (*9*). Another strategy is to use activatable cell-penetrating peptides conjugated to a quenched fluorophore (*10*). In general, these cathepsin- and MMP-activatable probes have been administered intravenously and accumulate preferentially in tumors owing to enhanced permeability and retention (EPR) (*9*, *11*). Activation of these enzyme-activatable probes is induced by enzymatic cleavage with endopeptidases; therefore, the unquenching process can extend from several hours to days before yielding sufficient signal above background in tumor sites.

Specific aminopeptidases are expressed at high levels in many cancers, such as hepatic cancer and glioma, and exhibit increased activity compared to normal sites (*12*), both in the local microenvironment and systemically. Among them, γ-glutamyltranspeptidase (GGT; Enzyme Commission number 2.3.2.2), a cell surface–associated (or bound) enzyme involved in cellular glutathione homeostasis, has been reported to be overexpressed in several human tumors, including those from cervical and ovarian cancers (*13*–*15*). It has been suggested that GGT promotes tumor progression, invasion, and drug resistance, possibly through modulation of intracellular redox metabolism (*16*). Despite its potential role in tumorigenesis, real-time imaging of GGT enzymatic activity in human cancer cells has not yet been reported in vitro or in vivo.

Here, we report a molecular imaging method for detecting cancer cells in vivo using a rationally developed fluorescence probe, γ-glutamyl hydroxymethyl rhodamine green (gGlu-HMRG), which is completely quenched by spirocyclic caging but is activated rapidly with a one-step enzymatic reaction in the presence of GGT. Topical application of the probe can be performed with lower doses than systemic administration. Furthermore, gGlu-HMRG can be sprayed onto tissue surfaces that are suspected of harboring tumors. Instant and complete activation of the probe makes it feasible for incorporation into surgical or endoscopic biopsy or resection procedures.

[1]Graduate School of Medicine, The University of Tokyo, Tokyo 113-0033, Japan. [2]Basic Research Program, Japan Science and Technology Agency, Tokyo 102-0075, Japan. [3]Graduate School of Pharmaceutical Science, The University of Tokyo, Tokyo 113-0033, Japan. [4]Molecular Imaging Program, Center for Cancer Research, National Cancer Institute, National Institutes of Health, Bethesda, MD 20892, USA. [5]Laboratory of Cancer Prevention, Center for Cancer Research, National Cancer Institute–Frederick, National Institutes of Health, Frederick, MD 21702, USA.
*To whom correspondence should be addressed. E-mail: kobayash@mail.nih.gov (H.K.); uranokun@m.u-tokyo.ac.jp (Y.U.)

RESULTS

Development of novel aminopeptidase-reactive fluorescent probes

GGT is bound to cell membranes and catalyzes the hydrolysis of the γ-glutamyl bond between glutamate and cysteine, the first step in the degradation of extracellular glutathione (GSH). The mechanism of visualizing GGT activity in living cells is shown in Fig. 1A. In serum, the gGlu-HMRG probe cannot permeate the plasma membrane because of its hydrophilicity. When gGlu-HMRG encounters GGT on the surface of a cancer cell, it is hydrolyzed by the enzyme to yield the highly fluorescent product, HMRG (Fig. 1A). HMRG, which is sufficiently hydrophobic, can permeate the lipid bilayer of the plasma membrane to enter cancer cells and accumulate mainly in lysosome (fig. S1). The kinetics of gGlu-HMRG in buffer were assessed for cleavage of GGT, compared with a control enzyme probe,

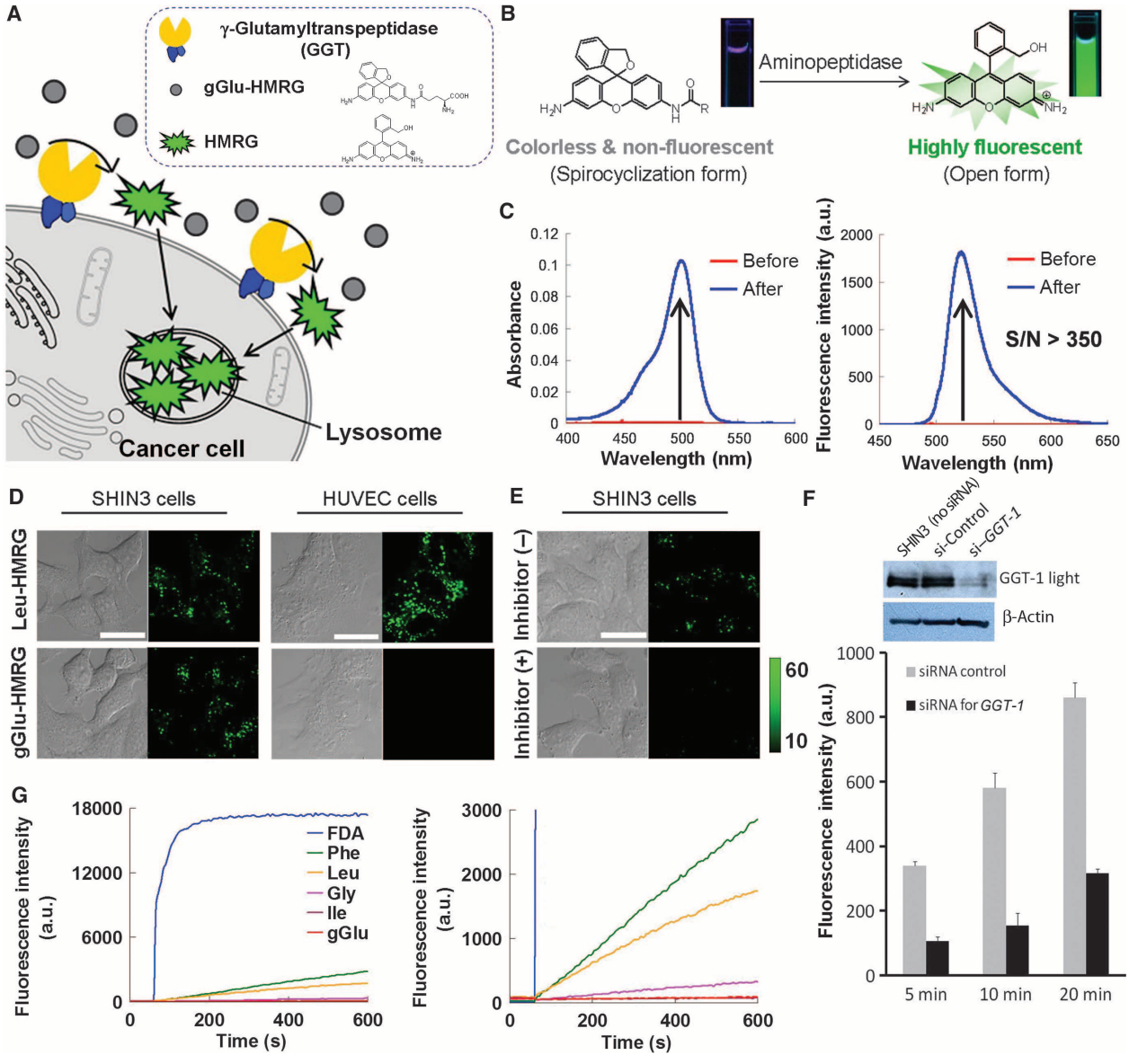

Fig. 1. The gGlu-HMRG probe is specifically activated by GGT and retained in cancer cells. (**A**) Proposed mechanism of gGlu-HMRG activation and retention. gGlu-HMRG reacts with up-regulated GGT anchored in the plasma membrane of cancer cells. This interaction enzymatically cleaves the probe to yield a highly fluorescent and membrane-permeable product, HMRG, which accumulates in the lysosomes of cancer cells. (**B**) Aminopeptidase-sensitive fluorescence probes containing HMRG, such as gGlu-HMRG, fluoresce in their uncaged forms. (**C**) Changes in absorbance and fluorescence of gGlu-HMRG upon reacting with GGT. S/N, signal-to-noise ratio; a.u., arbitrary units. (**D**) Comparison of GGT and LAP activities in human cancer cells (SHIN3) and normal cells (HUVEC) in response to respective enzyme-specific probes gGlu-HMRG and Leu-HMRG. Scale bars, 25 μm. (**E**) Inhibitory effect of GGsTop in SHIN3 cells with gGlu-HMRG. Scale bar, 25 μm. (**F**) siRNA knockdown of *GGT-1* in the SHIN3 cancer cells and activation of gGlu-HMRG. Data are mean fluorescence intensities (a.u.) ± SEM. (**G**) Stability of various aminopeptidase-activated probes and an esterase probe in 10% murine serum. The graph on the right is a magnified one of the graph on the left to show the difference in nonspecific activation of the aminopeptidase probes.

γ-glutamyl-3-carboxy-4-nitroanilide (gGlu-CNA), as well as the detection limits of GGT (fig. S2).

We have established recently a new design strategy based on the intramolecular spirocyclization with hydroxymethyl moiety (*17*). To detect enzymatic activities of various aminopeptidases in vivo, we applied this strategy to RG fluorophore to create HMRG scaffold, and by attaching various amino acids to one amino group of HMRG, we have developed five kinds of novel fluorescent probes—those bearing gGlu, leucyl (Leu), glycyl (Gly), isoleucyl (Ile), or phenylalanyl (Phe) moieties. These probes are nearly colorless and nonfluorescent at neutral pH owing to the preferred spirocyclized state, which results in light quenching (Fig. 1B). When hydrolyzed by their respective target enzymes, they yield highly fluorescent products (Fig. 1B) that can be imaged with visible light (~500 nm) (Fig. 1C).

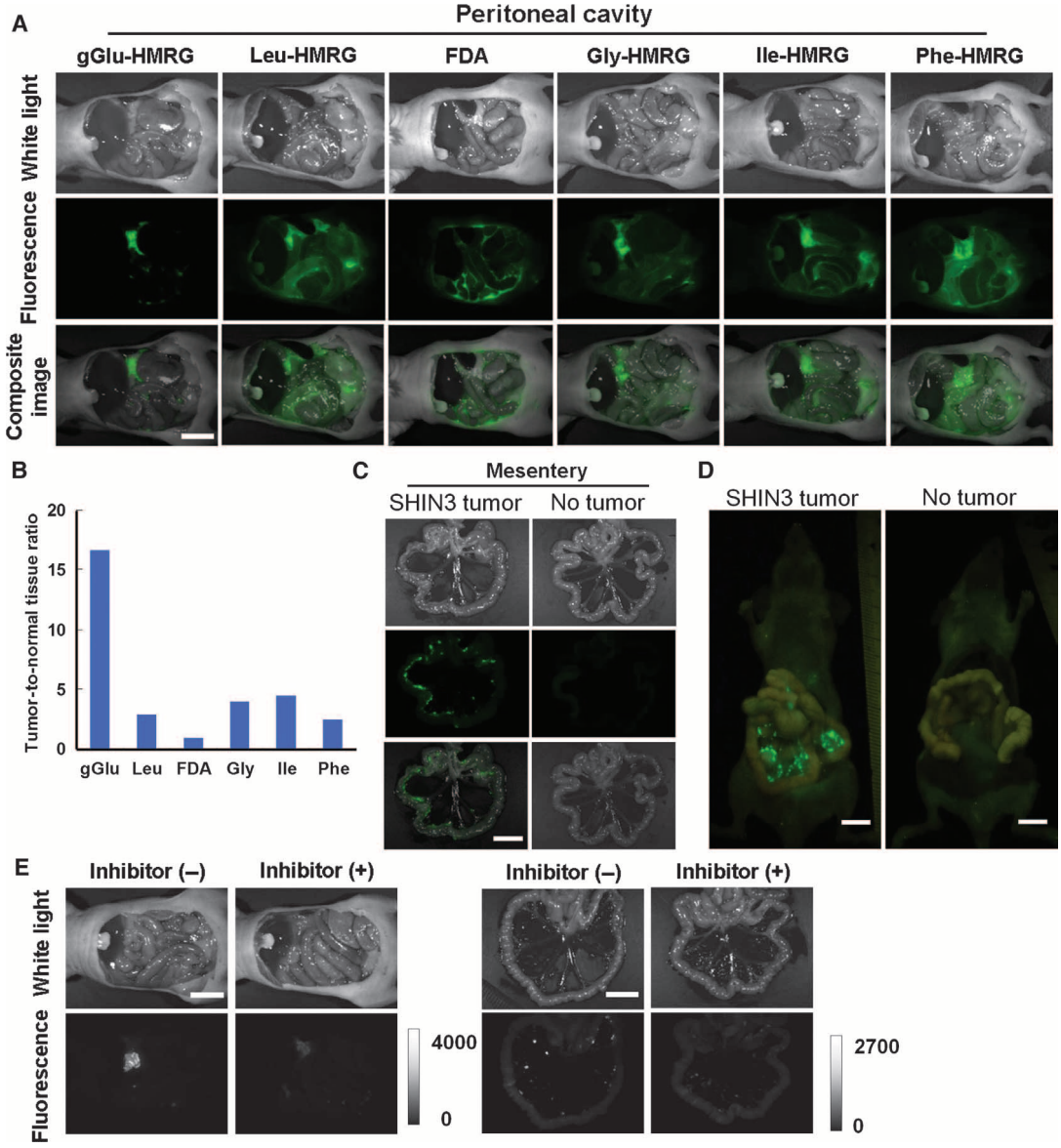

Fig. 2. gGlu-HMRG probe illuminated SHIN3 tumors with minimal background in vivo. (**A**) Representative white light, fluorescence, and composite images of the mouse peritoneum (representative of three to five mice per group) 10 min after intraperitoneal injection of gGlu-HMRG, Leu-HMRG, FDA, Gly-HMRG, Ile-HMRG, or Phe-HMRG in a SHIN3 mouse model of disseminated ovarian cancer. (**B**) Tumor–to–normal tissue ratio of fluorescence intensity in the peritoneal cavity of SHIN3-disseminated mice with various activatable probes. (**C**) Ex vivo fluorescence imaging of the spread mouse mesentery of tumor-bearing mice and control mice with gGlu-HMRG. Scale bar, 1 cm. (**D**) A fluorescence image of the peritoneal cavity 10 min after intraperitoneal injection of gGlu-HMRG into the SHIN3 mouse model and a non–tumor-bearing normal mouse. Scale bars, 1 cm. (**E**) White light and fluorescence images of mouse peritoneal cavity and mesentery 10 min after intraperitoneal injection of gGlu-HMRG, with (+) or without (–) co-injection of GGsTop inhibitor. Scale bars, 1 cm.

Evaluation of aminopeptidase activity and specificity in cancer cells

Our newly developed fluorescence probes for GGT and LAP (leucine aminopeptidase), which also has been reported as a tumor-associated enzyme (*18*)—gGlu-HMRG and Leu-HMRG, respectively—were applied to SHIN3 (human ovarian cancer) cells and HUVECs (human umbilical vein endothelial cells) as respective representative cancer cells and normal cells (Fig. 1D). GGT activity was successfully detected with gGlu-HMRG, and not with the conventional RG-based fluorescent probe with two reactive moieties, $(gGlu)_2$-RG, because it required cleavage of only one amide bond owing to the unique spirocyclic structure of the molecule, compared to the two amide bonds for $(gGlu)_2$-RG (fig. S3). GGT activity was higher for SHIN3 cancer cells compared with normal HUVECs, cleaving gGlu-HMRG to produce a fluorescent signal (Fig. 1D). However, LAP activity, detected with Leu-HMRG, did not differ between SHIN3 cells and HUVECs.

To show substrate selectivity of gGlu-HMRG for GGT only, we added GGsTop (*19*), a known inhibitor of GGT, to the cells, effectively blocking gGlu-HMRG fluorescence in SHIN3 cells (Fig. 1E). In addition, 95% of small interfering RNA (siRNA) silencing of the *GGT-1* gene induced a decrease in fluorescence ranging from 63 to 72% compared with an siRNA control at 5, 10, and

20 min after incubation (Fig. 1F), suggesting that GGT-1 is responsible for the activation and local accumulation of gGlu-HMRG.

Stability of fluorescence probes in serum

The stability of the fluorescent probes in serum, which contains several hydrolases, including peptidases, glycosidases, and esterases, was investigated by adding murine serum to a buffered solution of each aminopeptidase probe as well as a solution of fluorescein diacetate (FDA), an esterase-reactive probe, and measuring fluorescence over time (10 min) (Fig. 1G). High FDA activity was noted in serum. Among the five aminopeptidase probes, reactivities of Phe-, Leu-, and Gly-HMRG were found to be higher than those of gGlu- and Ile-HMRG, which were minimally hydrolyzed under these conditions (Fig. 1G). This indicates that the gGlu-HMRG probe would not be nonspecifically cleaved by other enzymes in vivo and would not produce a false-positive signal.

In vivo detection of SHIN3 tumor cells with gGlu-HMRG probe

To evaluate in vivo probe activation in the presence of cancer cells, we injected five aminopeptidase probes and FDA intraperitoneally into SHIN3 tumor–bearing mice. Mice were killed 10 min after injection, and fluorescent images were obtained. Rapid activation of Leu-HMRG and FDA and resulting fluorescence was observed not only at the tumor site but also in the background (Fig. 2A), which was consistent with their nonspecific activation in serum (Fig. 1G). Gly-, Ile-, and Phe-HMRG gave similar nonspecific results (Fig. 2A). Conversely, with the gGlu-HMRG probe, the tumor site was visualized within 10 min after probe injection with high TBR, which was much higher than relatively low TBR in the case of other probes (Fig. 2B). Tiny tumor sites less than 1 mm in diameter on the mesentery and peritoneal wall could be visualized (Fig. 2C). Furthermore, the fluorescence intensity of cancer cell–laden regions was high enough to be detected with the naked eye (Fig. 2D), which would be useful during surgical resection. Non–tumor-bearing normal mice injected with gGlu-HMRG did not show fluorescence (Fig. 2D), which indicated low background activity of GGT in both serum and normal cells. Furthermore, upon co-injection of the GGsTop inhibitor with gGlu-HMRG, we noticed minimal fluorescence in tumor sites in both the peritoneal cavity and the mesentery (Fig. 2E), which suggests that GGT activity is necessary for activating the probe in vivo.

Fluorescence detection of ovarian cancer cells in vitro and peritoneal tumors in vivo with gGlu-HMRG

To investigate the extent of GGT expression in ovarian cancer cell lines, we incubated gGlu-HMRG with 11 different human ovarian cancer cell lines in vitro (SHIN3, SKOV3, OVCAR3, OVCAR4, OVCAR5, OVCAR8, A2780, A2780 PTX22, IGR-OV1, Hey-A8, and CaOV3) and 6 different ovarian tumor implants in vivo (SHIN3, SKOV3, OVCAR3, OVCAR4, OVCAR5, and OVCAR8). All 11 ovarian cancer cell lines showed activation and accumulation of gGlu-HMRG probe by 60 min, which was confirmed with fluorescence microscopy and flow cytometry (Fig. 3).

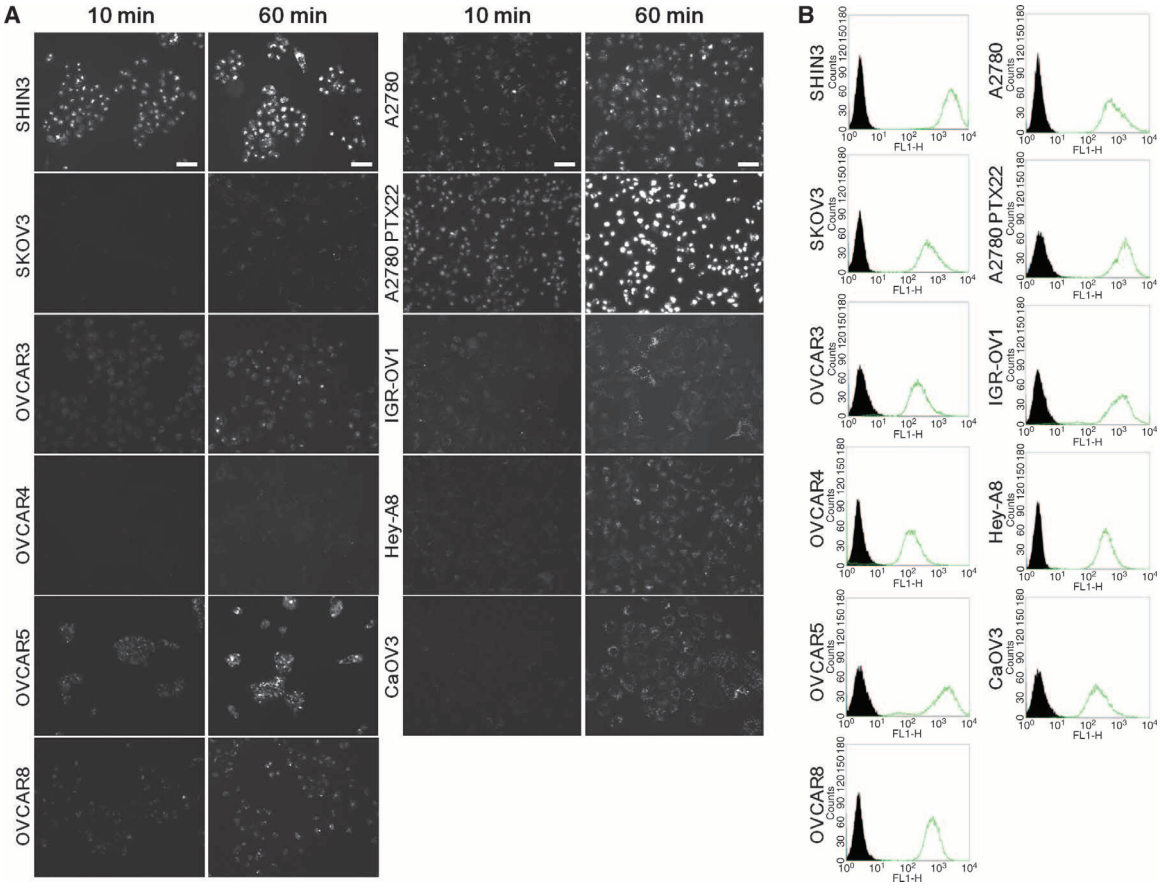

Fig. 3. gGlu-HMRG probe illuminates ovarian cancer cell lines in vitro. (**A** and **B**) Microscopic images of 11 human ovarian cancer cell lines 10 and 60 min after incubation (A) and flow cytometry results 60 min after incubation (B) with gGlu-HMRG. Scale bars, 50 μm.

Six of the 11 cell lines were chosen for in vivo study because the other 5 cell lines did not form peritoneal tumors in athymic mice. The endoscope was inserted into the abdominal cavity of living ovarian tumor–bearing, anesthetized mice through a small abdominal incision, and gGlu-HMRG probe diluted in phosphate-buffered saline (PBS)

was sprayed on the peritoneal surface with the endoscopic spray catheter that exactly simulated the clinical application in humans (for example, endoscopy with Lugol's solution administered by spray for detecting esophageal cancer or methylene blue for detecting early gastric or colon cancer), and activation was observed with a mini-endoscope fluorescence camera. Four of six peritoneal implants were detected within minutes after spraying the gGlu-HMRG probe, with significantly increasing fluorescence signal over the first 10 min ($P < 0.01$) (Fig. 4, A and B, and videos S1 to S7). These fluorescence intensity changes at 10 and 60 min observed with endoscopic study (Fig. 4B) were validated ex vivo by spectral fluorescence imaging of the abdominal cavity (Fig. 5). SKOV3 and OVCAR3 tumors were shown to be less bright than the pancreas, which showed weak physiological activation of the gGlu-HMRG probe.

In vitro cellular and in vivo tumor activation of the gGlu-HMRG probe was generally consistent in fluorescence intensity, except in one cell line, OVCAR4, which was not strongly activated by cells in vitro at 1 hour (Fig. 3A), but highly activated by the tumor in vivo by 10 min (Fig. 5 and video S4). OVCAR4 cells proliferated in culture very well with 1-day doubling time; however, these cells slowly produced peritoneal tumors for an average of 3 months compared with other cell lines that established peritoneal tumors within a month. This slow in vivo proliferation might concentrate GGT in the cell membrane. To support this hypothesis, a newly established cell line of OVCAR4, which was regenerated from a high GGT–expressing peritoneal tumor and proliferated similarly to the parental OVCAR4 cell line, showed similar GGT expression in in vitro culture to the parental OVCAR4 cells (fig. S4).

Finally, SHIN3 small nodules were sharply defined in the peritoneum as early as 30 s after spraying the gGlu-HMRG probe (Fig. 4C and video S1). Tiny implants (~1 mm in diameter) could be removed easily with forceps under fluorescence-guided endoscopy in living, anesthetized mice (Fig. 4D and video S8).

gGlu-HMRG for imaging small, peritoneally disseminated SHIN3 tumors

Red fluorescent protein (RFP)–transfected SHIN3 cells (SHIN3-RFP) were used for determining the sensitivity and specificity of detecting small (~1 mm) peritoneal ovarian cancer nodules with gGlu-HMRG injected intraperitoneally into mice. In the control experiments, no overlapping fluorescence was found between gGlu-HMRG and RFP (Fig. 6A). Mean nodule area on the RFP images was 0.68 ± 0.53 mm^2 (average ± SD, median 0.53 mm^2, minimum 0.079 mm^2, maximum 2.31 mm^2). Overlap of green and red fluorescence in tumor nodules was shown in microscopic (Fig. 6B) and spectral macroscopic (Fig. 6C) images only 10 min after injection of gGlu-HMRG into the peritoneum.

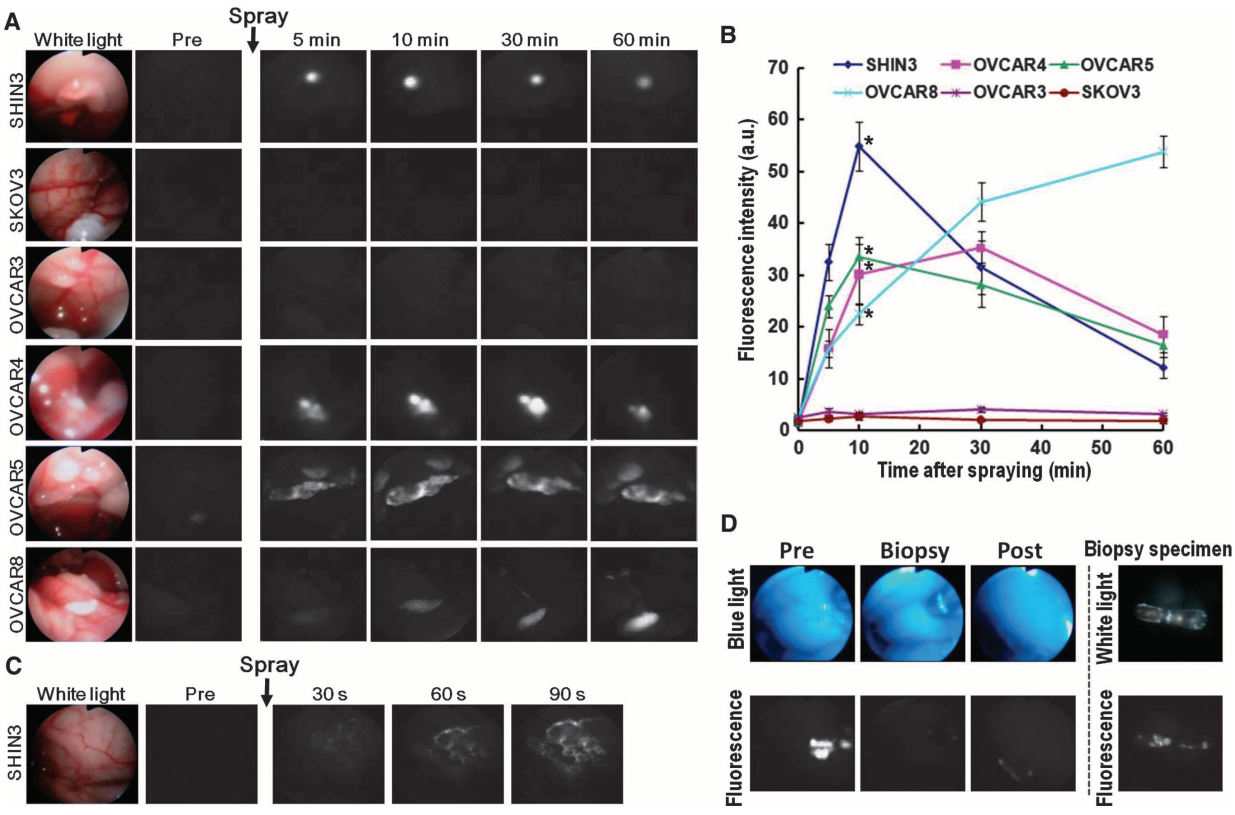

Fig. 4. gGlu-HMRG probe illuminates experimental tumors in vivo. (**A**) gGlu-HMRG fluorescence is detected endoscopically in implanted ovarian tumors in living mice over the course of 60 min (see videos S1 to S5 for ≤5 min after spraying gGlu-HMRG, and video S6 for 1 hour after spraying gGlu-HMRG). (**B**) Changes in tumor fluorescence signals in six ovarian cancer–bearing mice ($n = 4$ per group). Data are mean fluorescence intensities (a.u.) ± SEM of tumor nodule at different time points. Four of six peritoneal implants significantly increase in fluorescence signal over the first 10 min. *$P < 0.01$ compared to fluorescence signal immediately after spraying gGlu-HMRG, Wilcoxon matched-pairs test. (**C**) Within 90 s, gGlu-HMRG illuminates SHIN3 tumors growing in the mouse peritoneum (video S1). (**D**) Tiny ovarian cancer implants (~1 mm) were removed with forceps using fluorescence-guided endoscopy (video S8).

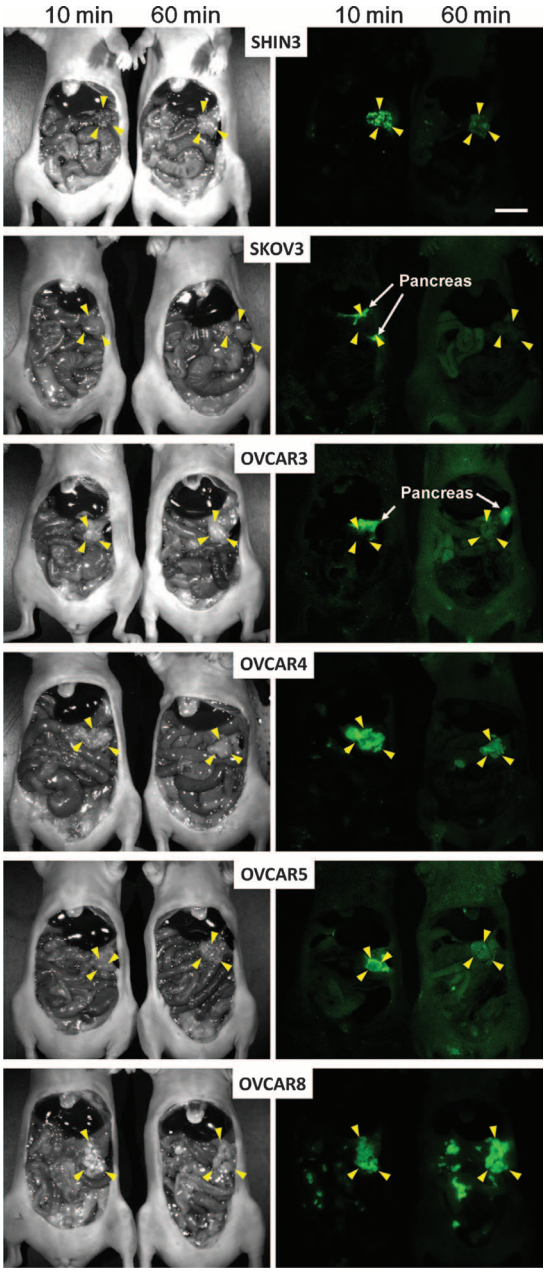

Fig. 5. Spectral fluorescence images of six peritoneal ovarian cancers confirm in vivo endoscopic imaging results. In vivo fluorescence intensity 10 and 60 min after intraperitoneal gGlu-HMRG administration was evaluated with six peritoneal ovarian tumor models: SHIN3, SKOV3, OVCAR3, OVCAR4, OVCAR5, and OVCAR8. After establishing the intraperitoneal dissemination model, one mouse from each pair (four pairs per cell line) was injected intraperitoneally with gGlu-HMRG. Yellow arrowheads indicate tumor location. White arrows indicate pancreas location. Scale bar, 1 cm.

Macroscopic coincidence of the two fluorescence signals counted as true-positive detection of tumor nodules and microscopic findings validated signal coincidence at the cellular level. When RFP was used as a reference for location of SHIN3 cells [10 arbitrary units (a.u.)] and the threshold of green fluorescence signal set at 4 a.u., sensitivity and specificity of detecting SHIN3-RFP tumors measuring about 1 mm in diameter (average 0.68 mm^2; n = 104) with gGlu-HMRG were 100 and 100%, respectively, at 10 min after injection (Fig. 6D).

DISCUSSION

GGT is overexpressed in various human cancer cell types in vivo (*13*–*15*) and is therefore considered to be a potential serum biomarker for early cancer detection. GGT activity has been examined previously in vitro with *p*-nitroanilide–based colorimetric assays (*20*) and the aminomethylcoumarin-based fluorescence assay (*21*); neither method was feasible for in vivo imaging because of the relatively low sensitivities of both methods and high autofluorescence in background, normal tissues. The use of $(gGlu)_2$-RG would avoid autofluorescence in vivo; however, a two-step hydrolyzation of both functional moieties is necessary to yield sufficient fluorescent signal, which renders these probes less sensitive. Indeed, GGT activity in SHIN3 cells could not be visualized with $(gGlu)_2$-RG under the same conditions as gGlu-HMRG probe. In contrast, our HMRG-based probes were rapidly and completely activated by their respective aminopeptidases, allowing near real-time visualization of aminopeptidase enzymatic activity.

Elevated expression of GGT has also been reported in patients with cervical intraepithelial neoplasia III and early stages of invasive cervical cancer (*22*). Colposcopic detection of early-stage uterine cervical cancer is a widely performed procedure; however, visual observation is still the most reliable method for directing painful biopsy even with many false negatives. Because a large proportion of cervical cancer purportedly expresses GGT, fluorescence guidance can assist to locate cancer and minimize painful sampling and false-negative cases.

Here, we report a gGlu-based probe in a class of HMRG molecules that can be used for detecting human cancer in vivo in an animal model. We have devised a solution that is amenable to spraying in vivo, thus interfacing more readily with intraoperative and endoscopic procedures. Although the design of GGT-activatable probe can be modified, current design of this gGlu-HMRG probe is the simplest. Shorter reaction steps will help keep the cost low and the yield high.

We propose that HMRG, which is hydrophobic, can be taken up by the cell in lysosomes, fluorescently labeling cancer cells internally. This proposed mechanism was supported in this study by administering GGsTop—a selective inhibitor of GGT that is highly hydrophilic and thought to exist only outside of the cells—in conjunction with the probe: No fluorescence was detectable in GGT-inhibited SHIN3 cells. The importance of GGT for enzymatically activating the gGlu-HMRG probe was verified with *GGT-1* knockdown in SHIN3 cancer cells. Furthermore, the enzymatic activity of GGT is high enough for yielding fluorescent product to see tumors even by the naked eye within seconds to minutes after spraying the probe directly on the peritoneal surface.

The rapidity of activation of gGlu-HMRG is an advantage of this probe. Most activatable probes, including ProSense and MMPSense (PerkinElmer Inc.) (*9*), and our own pH-activatable probes (*6*), take hours to days before a strong fluorescent signal compared to background can be seen. This long activation time hampers practical use of agents during surgical or endoscopic procedures. In contrast, gGlu-HMRG is activated within 10 min and will stay fluorescent for at least 1 hour, highlighting the tumor border. This amount of time is sufficient

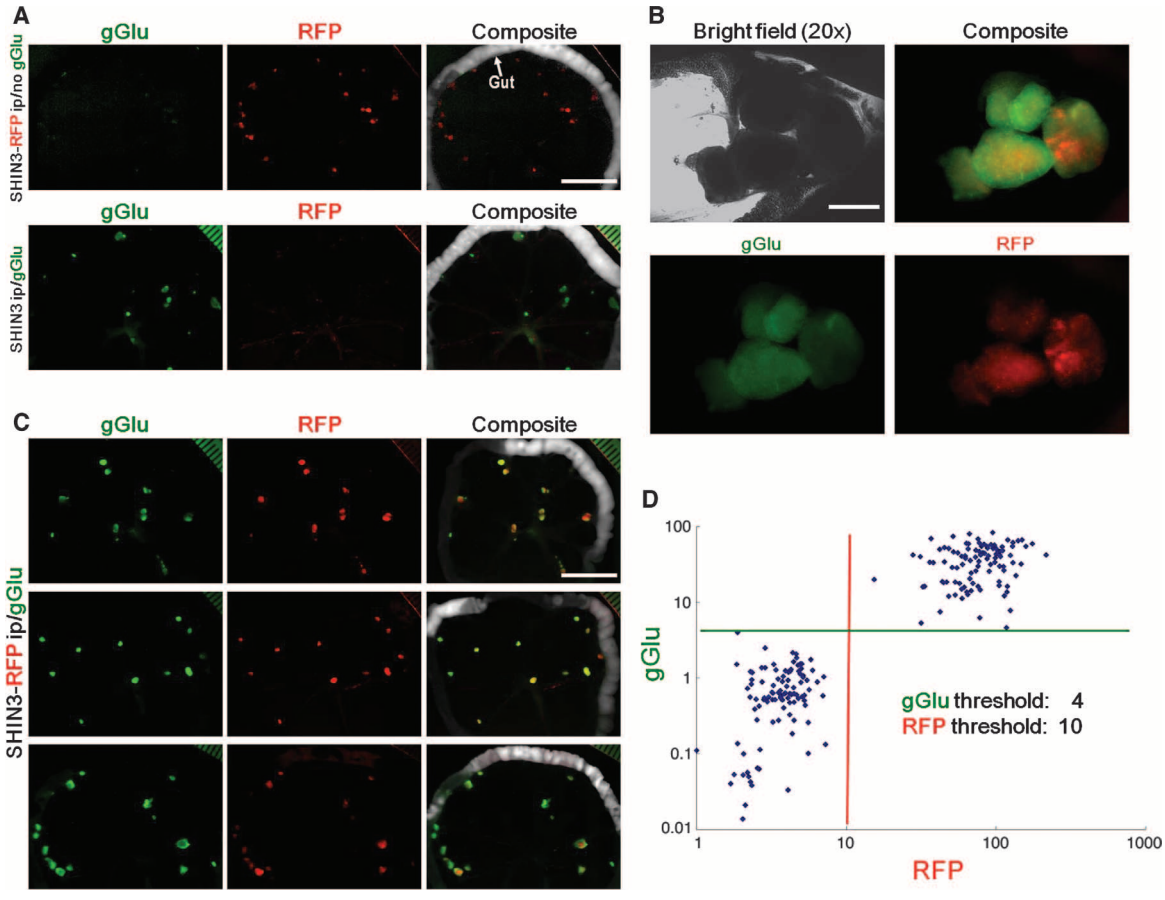

Fig. 6. Sensitivity and specificity of gGlu-HMRG for detecting tumors about 1 mm in diameter. (**A**) No crosstalk of fluorescence signals between gGlu-HMRG and RFP using parent SHIN3 tumors (no RFP) and SHIN3-RFP tumors. (**B** and **C**) Fluorescent imaging 10 min after intraperitoneal (ip) injection of the gGlu-HMRG probe: microscopic (fluorescence microscope) (B) and macroscopic (whole-body fluorescence imager) (C). Scale bars, 1 mm (B) and 1 cm (C). (**D**) Scatter plot of the fluorescence intensities in each nodule. When RFP was used as a reference for location of SHIN3 cells (10 a.u.) and the threshold of green fluorescence signal was set at 4 a.u., the sensitivity and specificity of detecting SHIN3-RFP tumors with gGlu-HMRG were 100 and 100%, respectively, 10 min after injection.

for performing many interventional procedures in the clinic, such as image-guided biopsy of gastrointestinal tract cancers or cervical cancer and fluorescence-guided laparoscopic surgery of peritoneal ovarian cancer metastases. The rapid activation of gGlu-HMRG enables topical administration with commensurate reductions in dose: Less than 1% of the probe is needed for topical application compared with the currently used intravenous dose of fluorescein (10 to 25 mg/kg) for angiographic application for visualizing the retinal vasculature in the clinical practice. The substantially lower dose required for topical administration via spraying compared to systemic intravenous administration likely reduces potential toxicity concerns for similar organic fluorophores, which have already been reported for human imaging (*23*).

In the current endoscopy system, the fluorescence images and standard endoscopy images were displayed separately. The practical limitation is that the surgeon might have to switch between bright-field and fluorescence modes frequently in the operating room to make use of the fluorescent probes. Additionally, the gGlu-HMRG probe might not be applicable to all types of cancer, as shown for SKOV3 or OVCAR3 tumors. Recent publications in this field indicate that, with proper excitation and emission filters, fluorescence laparoscopy can simultaneously visualize fluorescently labeled tumors and normal anatomy as seen by standard bright-field lighting (*24*, *25*). Furthermore, endoscopes and surgical cameras, which can magnify the objects with high sensitivity, might improve detection of tumors (<1 mm diameter) smaller than those we visualized in this study. A small human study for visualizing ovarian cancer with the folate-FITC (fluorescein isothiocyanate) probe has recently been reported (*26*). The folate-FITC is a simple always-on probe for binding to the membrane folate receptor; hence, there is no opportunity for signal amplification or suppression of background fluorescence to improve TBRs, which could reduce the sensitivity of the probe. By contrast, the gGlu-HMRG probe can theoretically yield higher tumor–to–normal tissue ratios than always-on probes.

The gGlu-HMRG probe could aid surgeons in detecting tiny cancerous nodules for accurate biopsy and tumor resection, delineating the borders of tumors for complete removal and confirming no residual tumor. Although GGT might not be a specific biomarker for all cancers, other probes similar to gGlu-HMRG can be developed for enzymes known to be located at the surface of tumors. Finally, the ability to topically apply the probe, coupled with the widespread use of optical cameras in the clinic, makes gGlu-HMRG attractive for screening human uterine cervical cancers.

MATERIALS AND METHODS

Materials and instruments

Reagents and solvents were supplied by Tokyo Chemical Industry, Wako Pure Chemical, or Aldrich Chemical Company, and were used without further purification. Dimethyl sulfoxide (DMSO; fluorometric grade) was used for spectrometric measurements (Dojindo).

Proton nuclear magnetic resonance (^{1}H NMR) and ^{13}C NMR spectra were recorded on JEOL JMN-LA300 and JMN-LA400 instruments. Mass spectra were measured with a JEOL JMS-T100LC AccuTOF. Ultraviolet (UV)–visible spectra were obtained on a Shimadzu UV-1650 (Supplementary Methods). Fluorescence spectroscopic studies were performed on a Hitachi F-4500. Serum assays in 96-well plates required a plate reader instrument coupled with a Corona SH-9000.

Detailed synthesis methods and analytical characterization of imaging probes (figs. S5 and S6 and table S1) are in the Supplementary Material.

Ninety-six–well plate serum assay

Experiments were performed on 96-well black plates (Nunc) at 37°C. Twenty microliters of murine serum was added to 180 μl of a 1.11 μM solution of FDA, Phe-HMRG, Leu-HMRG, Gly-HMRG, Ile-HMRG, or gGlu-HMRG in PBS (1 × PBS, pH 7.4). The plates were incubated for 30 min and fluorescence intensity was measured (excitation/emission, 490/520 nm).

Cell lines and culture

Eleven established human ovarian cancer cell lines were used in this study: SHIN3 (provided by S. Imai, Nara, Japan) (*27*); SKOV3 (*28*) and CaOV3 (American Type Culture Collection); A2780 and A2780 PTX22 [a gift from T. Fojo, National Cancer Institute, National Institutes of Health (NIH)]; Hey-A8 (a gift from G. Mills, M. D. Anderson Cancer Center); and OVCAR3, OVCAR4, OVCAR5, OVCAR8 (*29*), and IGR-OV1 (provided by the Developmental Therapeutics Program, National Cancer Institute–Frederick, NIH) (*30*). SHIN3 cells were transfected with a plasmid expressing RFP to create a red fluorescent phenotype (SHIN3-RFP), as described previously (*8*). All cell lines were grown in RPMI 1640 medium (Invitrogen) containing 10% fetal bovine serum (Invitrogen), 0.03% L-glutamine at 37°C, penicillin (100 U/ml), and streptomycin (100 μg/ml) in 5% CO_2.

siRNA knockdown of *GGT-1* in SHIN3 cells

To show specificity of gGlu-HMRG reacting with the GGT, we knocked down the gene *GGT-1* with siRNA (Silencer Select siRNA, Applied Biosystems). SHIN3 cells (5×10^5 total) were seeded in six-well dishes and transfected with 25 nM control siRNA (nonsense control; Applied Biosystems) (sense, UAACGACGCGACGACGUAATT; antisense, UUACGUCGUCGCGUCGUUATT) or *GGT-1*–targeted siRNA (sense, CCAAGGAACCUGACAACCAtt; antisense, UGGUUGUCAGGUUCCUUGGag) with DharmaFECT-1 (Dharmacon), according to the manufacturer's recommendations. Forty-eight hours after transfection, the gGlu-HMRG probe (2 μM) was added to the culture medium. The cells were incubated at 37°C and removed at 5, 10, or 20 min, and fluorescence was measured with a FLUOstar OPTIMA Fluorescence Microplate Reader (BMG Labtech; excitation/emission, 485/520 nm). *GGT-1* mRNA knockdown was confirmed by quantitative reverse transcription–polymerase chain reaction (RT-PCR) with the following primers for *GGT-1*: 5′-AATGGACGACTTCAGCTCTCC-3′ (forward) and 5′-AGCCGAACCAGAGGTTGTAGA-3′ (reverse). GGT protein levels were measured by immunoblotting with an anti–GGT-1 antibody (3E6; Santa Cruz Biotechnology).

In vitro fluorescence microscopy and flow cytometry

To compare fluorescence intensities of gGlu-HMRG and Leu-HMRG in vitro, we performed fluorescence microscopy with SHIN3 cells and HUVECs, 30 min after incubation with gGlu-HMRG and Leu-HMRG. For fluorescence microscopy, 4×10^4 cells from each cell line were plated on a cover glass–bottomed culture well and incubated at 37°C, in an atmosphere of 5% CO_2, for 2 days. gGlu-HMRG or Leu-HMRG (1 μM) was added to the culture medium and incubated for 30 min. Fluorescence images were captured with a Leica Application Suite Advanced Fluorescence (LAS-AF) microscope with a TCS SP5 and a 60× objective lens (excitation/emission, 501/510 to 540 nm).

To evaluate the time course of fluorescence intensities after gGlu-HMRG administration in vitro, we performed fluorescence microscopy and flow cytometry with all 11 ovarian cancer lines. For fluorescence microscopy, the same procedure was used as above with Leu-HMRG, except for alterations in the concentration of gGlu-HMRG (2 μM), incubation time (10 or 60 min), and the fluorescence microscope used (Olympus BX51 microscope, with Olympus band-pass filters from 470 to 490 nm and from 515 to 550 nm for excitation and emission, respectively). Transmitted light differential interference contrast (DIC) images were also acquired.

For flow cytometry, 1×10^5 cells from each cell line were plated in a six-chamber culture well and incubated for 16 hours. gGlu-HMRG (2 μM) was added to the culture medium, and the cells were incubated for 10 or 60 min. A 488-nm argon ion laser was used for excitation. Signals from cells were collected with a 515- to 545-nm band-pass filter. Cells were analyzed in a FACScan cytometer (Becton Dickinson), and all data were analyzed with CellQuest software (Becton Dickinson). The mean fluorescence intensity was determined in triplicate.

Tumor model of peritoneal implants

All procedures were carried out in compliance with the *Guide for the Care and Use of Laboratory Animal Resources* and the National Research Council, and were approved by the Institutional Animal Care and Use Committee of the NIH. Seven human ovarian cancer cell lines were used for in vivo studies: SHIN3, SHIN3-RFP, SKOV3, OVCAR3, OVCAR4, OVCAR5, and OVCAR8. The tumor implants were established by intraperitoneal injection of 1×10^6 to 2×10^6 cells suspended in 200 to 300 μl of PBS in female nude mice. Each cell line required different duration of time to produce multiple disseminated tumors of about 1 mm in size. Experiments with tumor-bearing mice were performed between 7 and 20 days for SHIN3, SHIN3-RFP, OVCAR5, and OVCAR8 models, between 35 and 45 days for SKOV3 and OVCAR3 models, and at 90 days for the OVCAR4 model, when disseminated peritoneal implants grew to about 1 mm in size.

In vivo spectral fluorescence imaging study

To evaluate the fluorescence intensities of gGlu-HMRG, Leu-HMRG, Gly-HMRG, Ile-HMRG, Phe-HMRG, and FDA in vivo, we performed spectral fluorescence imaging study with SHIN3 models, which consistently grew and produced implants in peritoneal space similar to those in ovarian cancer patients within 2 weeks in athymic mice, and expressed GGT, both in vitro and in vivo, 10 min after intraperitoneal injection of the probe.

Mice were injected intraperitoneally with 300 μl of a 100 μM probe solution. After 10 min, mice were killed with CO_2 and the abdominal cavities were exposed. Fluorescence images were obtained with the Maestro In-Vivo imaging system (CRi Inc.). The blue-filter setting (excitation, 445 to 490 nm; emission, 515 nm long-pass) was used. The tunable filter was automatically stepped in 10-nm increments, from 500 to 800 nm, while the camera sequentially captured images at each

wavelength interval. The spectral fluorescence images consisting of autofluorescence and HMRG spectra were unmixed for visual assessments with Maestro software.

To evaluate tumor–to–normal tissue ratio with various aminopeptidase probes, we drew regions of interest (ROIs) (average = 0.4 mm^2) within the tumor nodules and in the surrounding adjacent areas in the peritoneal cavity, and then we calculated the average fluorescence intensity of each ROI on the exported 540-nm fluorescence images by Maestro software. The number of ROIs drawn in the tumor nodules and the surrounding areas was 5. Tumor–to–normal tissue ratio value was calculated as average fluorescence intensity of tumor nodules divided by that of surrounding areas.

To evaluate the specific activity of GGT at the tumor site in vivo, we performed a spectral fluorescence imaging study with one SHIN3 peritoneal agent–dissemination model mouse, which was injected intraperitoneally with 300 μl of a mixed PBS solution of 50 μM gGlu-HMRG and 50 μM GGsTop. To evaluate fluorescence intensity of gGlu-HMRG at 10 and 60 min after injection in vivo, we performed a spectral fluorescence imaging study with six peritoneal dissemination models (SHIN3, SKOV3, OVCAR3, OVCAR4, OVCAR5, and OVCAR8) at 10 and 60 min after gGlu-HMRG administration.

In vivo real-time fluorescence endoscopy study

To determine how rapidly gGlu-HMRG became activated in vivo, we performed fluorescence imaging during endoscopy in six of the peritoneal dissemination models (SHIN3, SKOV3, OVCAR3, OVCAR4, OVCAR5, and OVCAR8; $n = 4$ each). A clinical endoscopic system (Evis Exera-II CLV-180, Olympus Corp.) equipped with an in house–developed fluorescence detection system was used for this study, as described previously (*31*). Excitation and emission filters were 464.5 to 499.5 nm and 516 to 556 nm, respectively.

Mice were anesthetized via intravenous injection of 1.15 mg of sodium pentobarbital (Nembutal Sodium Solution, Ovation Pharmaceuticals Inc.). The endoscope was inserted into abdominal cavity through a small abdominal incision, and the abdominal cavity was inflated with air. After obtaining initial fluorescence images of the peritoneal surface, we diluted a gGlu-HMRG stock solution in DMSO with PBS to generate a 50 μM gGlu-HMRG spraying solution. Three hundred microliters of this solution was sprayed on the surface with the endoscopic spray catheter. Real-time fluorescence images of disseminated nodules were recorded for up to 60 min. Fluorescence images of 8 to 10 disseminated tumor nodules in each group were captured at 0, 10, 30, and 60 min, and subjected to semiquantitative analyses. Circular ROIs were placed in the center of the tumor nodules and adjacent backgrounds, fluorescence intensity of tumor nodules and backgrounds was measured with ImageJ software (NIH), and TBRs were calculated for each nodule. For large nodules, two ROIs were used to cover the entire area.

Sensitivity and specificity of gGlu-HMRG for the detection of peritoneal cancer implants

The sensitivity and specificity of gGlu-HMRG for the detection of cancer foci were studied with SHIN3-RFP tumor–bearing mice ($n = 7$), as described previously (*8*, *32*). Ten minutes after intraperitoneal injection of 300 μl of 25 μM gGlu-HMRG in PBS, mice were killed with CO_2 and the peritoneal membranes were incised and spread out on a nonfluorescent plate. High spatial resolution spectral fluorescence imaging using the maximum magnified setting was performed with the Maestro In-Vivo Imaging System and multiexcitation acquisition (blue filter: excitation, 445 to 490 nm; emission, 515 nm long-pass; yellow filter: excitation, 575 to 605 nm; emission, 645 nm long-pass) (*33*). The tunable filter was automatically stepped in 10-nm increments from 500 to 800 nm while the camera sequentially captured images at each wavelength interval. The spectral fluorescence images consisting of autofluorescence, RFP, and gGlu-HMRG spectra were unmixed for further analyses with Maestro software.

ROIs were drawn within the tumor nodules depicted by the RFP images (cancer foci: average fluorescence intensity ≥10 a.u.) and in the surrounding adjacent areas (noncancerous foci: average fluorescence intensity <10 a.u.), and then the average fluorescence intensity of each ROI was calculated on the gGlu-HMRG images with ImageJ software. The number of ROIs drawn in the noncancerous areas was equal to the number drawn on cancer foci ($n = 104$). All visible nodules with areas >0.05 mm^2 on RFP images were analyzed. Additional ROIs were drawn on the nodules depicted on the gGlu-HMRG images and compared to the RFP images to validate the existence of SHIN3 tumors. The average fluorescence intensities of false-positive foci were calculated on both the RFP and the gGlu-HMRG unmixed images. Positive signal for gGlu-HMRG was defined as an average fluorescence intensity greater than 4 a.u.; a negative signal was defined as less than 4 a.u. The number of foci positive for both gGlu-HMRG and RFP, negative for both gGlu-HMRG and RFP, and positive only for gGlu-HMRG or RFP was counted. Sensitivity of gGlu-HMRG for the detection of peritoneal cancer foci was defined as the number of peritoneal foci that were positive for both gGlu-HMRG and RFP divided by the number of peritoneal foci positive for RFP. Specificity of gGlu-HMRG was defined as the number of peritoneal foci negative for both RFP and gGlu-HMRG divided by the number of peritoneal foci negative for RFP.

Statistical analysis

Statistical analysis was performed with a statistics program (GraphPad Instat, version 3.06, GraphPad Software). Wilcoxon matched-pairs test was used to compare the fluorescence signal changes from 0 to 10 min in the in vivo dynamic endoscopic study. Values of $P < 0.01$ were considered to be statistically significant.

SUPPLEMENTARY MATERIAL

www.sciencetranslationalmedicine.org/cgi/content/full/3/110/110ra119/DC1

Methods

Fig. S1. Fluorescence confocal imaging of SHIN3 cells loaded with HMRG and LysoTracker Red.

Fig. S2. Kinetic characteristics of gGlu-HMRG compared with gGlu-CNA.

Fig. S3. Comparison of gGlu-HMRG and $(gGlu)_2$-RG in SHIN3 cells.

Fig. S4. GGT activity of a regenerated cell line from a high GGT–expressing OVCAR4 peritoneal tumor.

Fig. S5. ^1H NMR trace of the gGlu-HMRG probe.

Fig. S6. Reversed-phase high-performance liquid chromatography (HPLC) chromatogram of five aminopeptidase probes.

Table S1. Optical characteristics of five aminopeptidase probes.

Video S1. Dynamic fluorescence endoscopy of SHIN3 metastases.

Video S2. Dynamic fluorescence endoscopy of SKOV3 metastases.

Video S3. Dynamic fluorescence endoscopy of OVCAR3 metastases.

Video S4. Dynamic fluorescence endoscopy of OVCAR4 metastases.

Video S5. Dynamic fluorescence endoscopy of OVCAR5 metastases.

Video S6. Dynamic fluorescence endoscopy of OVCAR8 metastases.

Video S7. Fluorescence endoscopy of six ovarian cancer metastases 60 min after spraying the gGlu-HMRG probe.

Video S8. Dynamic fluorescence endoscopy–guided biopsy of tiny peritoneal SHIN3 ovarian metastases.

REFERENCES AND NOTES

1. J. V. Frangioni, New technologies for human cancer imaging. *J. Clin. Oncol.* **26**, 4012–4021 (2008).
2. M. B. Wallace, R. Kiesslich, Advances in endoscopic imaging of colorectal neoplasia. *Gastroenterology* **138**, 2140–2150 (2010).
3. R. Weissleder, M. J. Pittet, Imaging in the era of molecular oncology. *Nature* **452**, 580–589 (2008).
4. H. Kobayashi, M. Ogawa, R. Alford, P. L. Choyke, Y. Urano, New strategies for fluorescent probe design in medical diagnostic imaging. *Chem. Rev.* **110**, 2620–2640 (2010).
5. H. Kobayashi, P. L. Choyke, Target-cancer-cell-specific activatable fluorescence imaging probes: Rational design and in vivo applications. *Acc. Chem. Res.* **44**, 83–90 (2011).
6. Y. Urano, D. Asanuma, Y. Hama, Y. Koyama, T. Barrett, M. Kamiya, T. Nagano, T. Watanabe, A. Hasegawa, P. L. Choyke, H. Kobayashi, Selective molecular imaging of viable cancer cells with pH-activatable fluorescence probes. *Nat. Med.* **15**, 104–109 (2009).
7. M. Ogawa, N. Kosaka, P. L. Choyke, H. Kobayashi, In vivo molecular imaging of cancer with a quenching near-infrared fluorescent probe using conjugates of monoclonal antibodies and indocyanine green. *Cancer Res.* **69**, 1268–1272 (2009).
8. Y. Hama, Y. Urano, Y. Koyama, M. Kamiya, M. Bernardo, R. S. Paik, I. S. Shin, C. H. Paik, P. L. Choyke, H. Kobayashi, A target cell–specific activatable fluorescence probe for in vivo molecular imaging of cancer based on a self-quenched avidin-rhodamine conjugate. *Cancer Res.* **67**, 2791–2799 (2007).
9. R. Weissleder, C. H. Tung, U. Mahmood, A. Bogdanov Jr., In vivo imaging of tumors with protease-activated near-infrared fluorescent probes. *Nat. Biotechnol.* **17**, 375–378 (1999).
10. E. S. Olson, T. A. Aguilera, T. Jiang, L. G. Ellies, Q. T. Nguyen, E. H. Wong, L. A. Gross, R. Y. Tsien, In vivo characterization of activatable cell penetrating peptides for targeting protease activity in cancer. *Integr. Biol.* **1**, 382–393 (2009).
11. U. Mahmood, C. H. Tung, A. Bogdanov Jr., R. Weissleder, Near-infrared optical imaging of protease activity for tumor detection. *Radiology* **213**, 866–870 (1999).
12. J. Stremenova, E. Krepela, V. Mares, J. Trim, V. Dbaly, J. Marek, Z. Vanickova, V. Lisa, C. Yea, A. Sedo, Expression and enzymatic activity of dipeptidyl peptidase-IV in human astrocytic tumours are associated with tumour grade. *Int. J. Oncol.* **31**, 785–792 (2007).
13. M. H. Hanigan, H. F. Frierson Jr., J. E. Brown, M. A. Lovell, P. T. Taylor, Human ovarian tumors express γ-glutamyl transpeptidase. *Cancer Res.* **54**, 286–290 (1994).
14. D. Yao, D. Jiang, Z. Huang, J. Lu, Q. Tao, Z. Yu, X. Meng, Abnormal expression of hepatoma specific γ-glutamyl transferase and alteration of γ-glutamyl transferase gene methylation status in patients with hepatocellular carcinoma. *Cancer* **88**, 761–769 (2000).
15. C. Schäfer, C. Fels, M. Brucke, H. J. Holzhausen, H. Bahn, M. Wellman, A. Visvikis, P. Fischer, N. G. Rainov, γ-Glutamyl transferase expression in higher-grade astrocytic glioma. *Acta Oncol.* **40**, 529–535 (2001).
16. A. Pompella, V. De Tata, A. Paolicchi, F. Zunino, Expression of γ-glutamyltransferase in cancer cells and its significance in drug resistance. *Biochem. Pharmacol.* **71**, 231–238 (2006).
17. M. Kamiya, D. Asanuma, E. Kuranaga, A. Takeishi, M. Sakabe, M. Miura, T. Nagano, Y. Urano, β-Galactosidase fluorescence probe with improved cellular accumulation based on a spirocyclized rhodol scaffold. *J. Am. Chem. Soc.* **133**, 12960–12963 (2011).
18. S. Mizutani, K. Shibata, F. Kikkawa, A. Hattori, M. Tsujimoto, M. Ishii, H. Kobayashi, Essential role of placental leucine aminopeptidase in gynecologic malignancy. *Expert Opin. Ther. Targets* **11**, 453–461 (2007).
19. L. Han, J. Hiratake, A. Kamiyama, K. Sakata, Design, synthesis, and evaluation of γ-phosphono diester analogues of glutamate as highly potent inhibitors and active site probes of γ-glutamyl transpeptidase. *Biochemistry* **46**, 1432–1447 (2007).
20. F. Schiele, Y. Artur, D. Bagrel, C. Petitclerc, G. Siest, Measurement of plasma gamma-glutamyltransferase in clinical chemistry: Kinetic basis and standardisation propositions. *Clin. Chim. Acta* **112**, 187–195 (1981).
21. E. Prusak, M. Siewinski, A. Szewczuk, A new fluorimetric method for the determination of γ-glutamyltransferase activity in blood serum. *Clin. Chim. Acta* **107**, 21–26 (1980).
22. A. M. Strasak, G. Goebel, H. Concin, R. M. Pfeiffer, L. J. Brant, G. Nagel, W. Oberaigner, N. Concin, G. Diem, E. Ruttmann, U. Gruber-Moesenbacher, F. Offner, A. Pompella, K. P. Pfeiffer, H. Ulmer; VHM&PP Study Group, Prospective study of the association of serum γ-glutamyltransferase with cervical intraepithelial neoplasia III and invasive cervical cancer. *Cancer Res.* **70**, 3586–3593 (2010).
23. R. Alford, H. M. Simpson, J. Duberman, G. C. Hill, M. Ogawa, C. Regino, H. Kobayashi, P. L. Choyke, Toxicity of organic fluorophores used in molecular imaging: Literature review. *Mol. Imaging* **8**, 341–354 (2009).
24. H. S. Tran Cao, S. Kaushal, C. Lee, C. S. Snyder, K. J. Thompson, S. Horgan, M. A. Talamini, R. M. Hoffman, M. Bouvet, Fluorescence laparoscopy imaging of pancreatic tumor progression in an orthotopic mouse model. *Surg. Endosc.* **25**, 48–54 (2011).
25. H. S. Tran Cao, S. Kaushal, R. S. Menen, C. A. Metildi, C. Lee, C. S. Snyder, M. A. Talamini, R. M. Hoffman, M. Bouvet, Submillimeter-resolution fluorescence laparoscopy of pancreatic cancer in a carcinomatosis mouse model visualizes metastases not seen with standard laparoscopy. *J. Laparoendosc. Adv. Surg. Tech. A* **21**, 485–489 (2011).
26. G. M. van Dam, G. Themelis, L. M. Crane, N. J. Harlaar, R. G. Pleijhuis, W. Kelder, A. Sarantopoulos, J. S. de Jong, H. J. Arts, A. G. van der Zee, J. Bart, P. S. Low, V. Ntziachristos, Intraoperative tumor-specific fluorescence imaging in ovarian cancer by folate receptor-α targeting: First in-human results. *Nat. Med.* **17**, 1315–1319 (2011).
27. S. Imai, Y. Kiyozuka, H. Maeda, T. Noda, H. L. Hosick, Establishment and characterization of a human ovarian serous cystadenocarcinoma cell line that produces the tumor markers CA-125 and tissue polypeptide antigen. *Oncology* **47**, 177–184 (1990).
28. M. C. Hung, X. Zhang, D. H. Yan, H. Z. Zhang, G. P. He, T. Q. Zhang, D. R. Shi, Aberrant expression of the *c-erbB-2/neu* protooncogene in ovarian cancer. *Cancer Lett.* **61**, 95–103 (1992).
29. T. C. Hamilton, R. C. Young, R. F. Ozols, Experimental model systems of ovarian cancer: Applications to the design and evaluation of new treatment approaches. *Semin. Oncol.* **11**, 285–298 (1984).
30. J. Bénard, J. Da Silva, M. C. De Blois, P. Boyer, P. Duvillard, E. Chiric, G. Riou, Characterization of a human ovarian adenocarcinoma line, IGROV1, in tissue culture and in nude mice. *Cancer Res.* **45**, 4970–4979 (1985).
31. M. Mitsunaga, N. Kosaka, R. C. Kines, J. N. Roberts, D. R. Lowy, J. T. Schiller, Y. Ishihara, A. Hasegawa, P. L. Choyke, H. Kobayashi, In vivo longitudinal imaging of experimental human papillomavirus infection in mice with a multicolor fluorescence mini-endoscopy system. *Cancer Prev. Res.* **4**, 767–773 (2011).
32. Y. Hama, Y. Urano, Y. Koyama, A. J. Gunn, P. L. Choyke, H. Kobayashi, A self-quenched galactosamine-serum albumin-rhodamineX conjugate: A "smart" fluorescent molecular imaging probe synthesized with clinically applicable material for detecting peritoneal ovarian cancer metastases. *Clin. Cancer Res.* **13**, 6335–6343 (2007).
33. Y. Koyama, T. Barrett, Y. Hama, G. Ravizzini, P. L. Choyke, H. Kobayashi, In vivo molecular imaging to diagnose and subtype tumors through receptor-targeted optically labeled monoclonal antibodies. *Neoplasia* **9**, 1021–1029 (2007).

Funding: This research was supported by the Intramural Research Program of the U.S. NIH, National Cancer Institute, Center for Cancer Research. This work was also financially supported by the Ministry of Education, Culture, Sports, Science and Technology of Japan (grants 23249004, 20117003, and 19205021 to Y.U.). **Author contributions:** M.S. and N.K. conducted experiments, performed analyses, and wrote the manuscript. M.O., M.M., D.A., M.K., and M.R.Y. conducted experiments and performed analysis. T.N. and P.L.C. wrote the manuscript and supervised the project. Y.U. and H.K. planned and initiated the project, designed and conducted experiments, wrote the manuscript, and supervised the entire project. **Competing interests:** The authors declare that they have no competing interests. We have filed two patents (PCT/JP2010/001077 and PCT/JP2011/050299).

Submitted 27 June 2011
Accepted 1 November 2011
Published 23 November 2011
10.1126/scitranslmed.3002823

Citation: Y. Urano, M. Sakabe, N. Kosaka, M. Ogawa, M. Mitsunaga, D. Asanuma, M. Kamiya, M. R. Young, T. Nagano, P. L. Choyke, H. Kobayashi, Rapid cancer detection by topically spraying a γ-glutamyltranspeptidase–activated fluorescent probe. *Sci. Transl. Med.* **3**, 110ra119 (2011).